Automobile Laminated Glass Window Embedded Transmitarray and Ray Tracing Validation for Enhanced 5G Connectivity

Seokyeon Hong, *Member, IEEE*, Yongwan Kim, *Member, IEEE*, and Jungsuek Oh, *Senior Member, IEEE*

***Abstract*— This article presents a 38.5 GHz transmitarray, for the first time, embedded into laminated car glass, and indoor 5G connectivity enhanced by this transmitarray laminated glass has also been validated using a ray-tracing simulator. The transmitarray structure reduces the penetration loss and realizes a desired beam shaping function. Metallic layers of the transmitarray structure adopt the Jerusalem cross shape that minimizes opacity. A ray-tracing simulator was used to analyze electromagnetic fields in a massive space, such as the interior of a car. The proposed transmitarray laminated glass was applied to the passenger side window in the simulation, and the variation in the communication performance with and without the transmitarray was compared. This comparison confirmed that field intensity increases of up to approximately 5 dB are realized at the target area, where communication is mainly performed. In addition, the proposed transmitarray laminated glass increases the field intensity by more than 3 dB, from approximately 36 to 40 GHz. The transmitarray laminated glass has also been fabricated. The maximum field intensity increase of approximately 5 dB, which is similar to the simulation results, was successfully measured at the target area.**

***Index Terms*— Metasurface, millimeter-wave propagation, ray tracing, transmitarray, vehicles.**

I. Introduction

COMPARED to the long-term evolution (LTE) mobile communication technology currently used, 5G mobile communication using millimeter-wave bands shows very weak performance under the nonline-of-sight (NLOS) condition [1]–[3]. To solve this problem, NTT and DOCOMO teamed up to demonstrate metastructure reflect-array technology. In addition, to solve the loss caused in the transmission of signals from outdoors to indoors, Samsung introduced an electronic product called customer-premises equipment (CPE) that acts as a repeater to amplify the external signal and radiate it inside the building. However, these coverage enhancements come with a considerable cost for additional electronic devices.

This article proposes the use of laminated glass with a transmitarray as the solution for high penetration loss in the millimeter wavelength band. There are many papers describing the implementation of frequency-selective surface (FSS) characteristics using a patterned structure of metal on a single glass layer [4]–[6]. In this article, however, the intent is to improve communication performance by incorporating metallic layers into a glass structure that serves as a double glass or a laminated glass. The work is intended for the automobile interior, among other interior environments. The transmitarray is applied to the laminated glass structure used in the vehicle, which improves the communication performance inside the vehicle by using the FSS and phase-shifting surface (PSS) characteristics. FSS characteristics change frequency response to minimize penetration losses at specific frequencies. PSS characteristics shape the beam through phase variation, which focuses the signal into the spatial domain where communication occurs frequently [7]. In 5G communication, fields that reach the space where communication does not occur undergo significantly large attenuation by large path loss, which is a natural property of the mm-wave. The energy of these fields cannot be used. Therefore, the PSS property is very important to ensure that most of the energy is delivered to the space, where communication occurs frequently. The target frequency is 38.5 GHz, which exhibits the highest penetration loss in the 5G millimeter waveband. The target area is the headrest portion of a seat, where communication devices in user's hand are mainly located when communication occurs.

In Section II, we probe the transmission characteristics of the vehicle laminated glass and relate the frequency and penetration loss (in the millimeter waveband) caused by the laminated glass. In Section III, the high-frequency structure simulator (HFSS) simulation tool is used to identify the unit cell (UC) structure of the transmitarray to be inserted into the laminated glass of the vehicle, and we check the beam shaping performance of the transmitarray consisting of seven types of UCs. Section IV introduces the use of the ray-tracing simulation to analyze the proposed transmitarray's propagation characteristics inside the vehicle when it is in the passenger side window [8]. In addition, the characteristics of the material and the experimental environment inside the vehicle are

Manuscript received 13 July 2021; revised 18 January 2022; accepted 21 February 2022. Date of publication 28 March 2022; date of current version 8 September 2022. This work was supported by the Institute of Information and Communications Technology Planning and Evaluation (IITP) grant funded by the South Korean Government [Ministry of Science and ICT (MSIT)] (in part by Advanced and Integrated Software Development for Electromagnetic Analysis under Grant 2019-0-00098 and in part by Innovative Fusion Technologies of Intelligent Antenna Material/Structure/Network for THz 6G under Grant 2021-0-00763). *(Corresponding author: Jungsuek Oh.)*

The authors are with the Institute of New Media and Communications (INMC) and the Department of Electrical and Computer Engineering, Seoul National University, Seoul 08826, South Korea (e-mail: syhong116@snu.ac.kr; yongwankim@snu.ac.kr; jungsuek@snu.ac.kr).

Color versions of one or more figures in this article are available at https://doi.org/10.1109/TAP.2022.3161432.

Digital Object Identifier 10.1109/TAP.2022.3161432

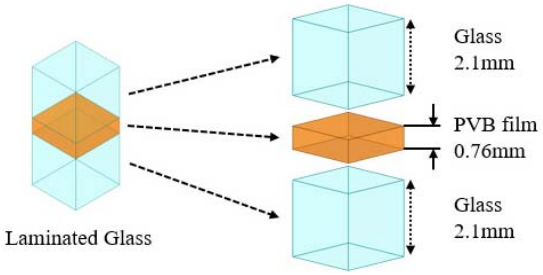

Fig. 1. Conventional automotive laminated glass structure used in actual car windows.

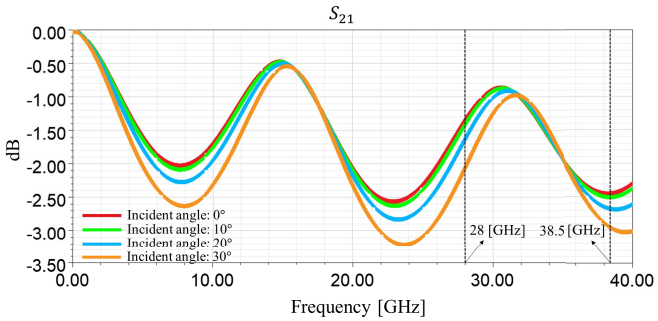

Fig. 2. Frequency response of the conventional automotive laminated glass shown in Fig. 1, for TE-polarization plane wave incidence.

TABLE I

IL OF CONVENTIONAL AUTOMOTIVE LAMINATED GLASS IN FIG. 1 AT 28 AND 38.5 GHz OVER SEVERAL INCIDENT ANGLES

INCIDENT ANGLE [°] (TE-POL)	IL [dB]	
	28 GHz	38.5 GHz
0	1.36	2.45
10	1.42	2.51
20	1.64	2.69
30	2.07	2.97

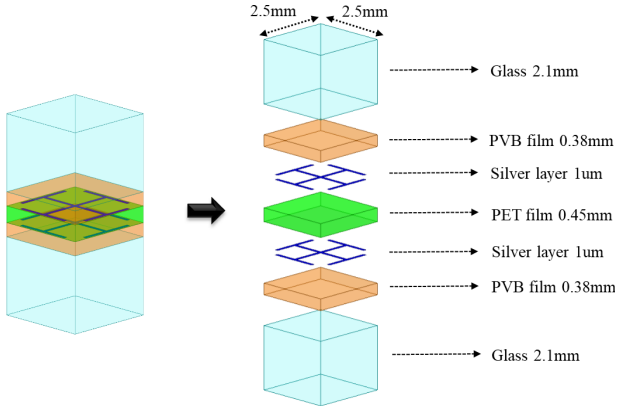

Fig. 3. Geometry of the proposed UC.

introduced. Finally, in Section V, the field intensity increases at the target area produced by the fabricated transmitarray laminated glass are shown and these are compared with the results of the ray-tracing simulation.

II. FREQUENCY RESPONSE OF CONVENTIONAL AUTOMOTIVE LAMINATED GLASS

Fig. 1 shows the structure of convectional laminated glass used in real vehicles. Conventional automotive laminated glass consists of two pieces of 2.1 mm glass and one piece of 0.76 mm polyvinyl butyral (PVB) film. PVB is a resin that is widely used for automotive laminated glass. Conventional automotive laminated glass is manufactured by inserting a PVB film into two sheets of glass, preventing the glass from breaking or scattering sharply. Fig. 2 shows the frequency response, calculated using HFSS simulation of conventional automotive laminated glass shown in Fig. 1 at several incident angles over different frequencies for TE-polarization plane wave incidence. The dielectric constant, loss tangent of the glass, and PVB film are 4.7, 0.03, and 3.6, 0.01, respectively. These properties are applied to the simulation. The frequency response S_{21} has a periodicity and the loss overall increases as the frequency increases. Also, due to the natural property of the TE-polarization for general planar interfaces, the overall insertion loss (IL) increases with incident angle. The conventional automotive laminated glass shows high penetration losses at the 5G mobile communication frequency band and a higher loss at 38.5 GHz than at 28 GHz. Table I shows the IL of conventional automotive laminated glass at 28 and 38.5 GHz, as a function of several incident angles. In this study, we seek a solution to the high penetration loss in the 38.5 GHz band of conventional automotive laminated glass.

III. DESIGN OF TRANSMITARRAY LAMINATED GLASS

A. Proposed Design of Unit Cells

In this study, we propose the insertion of a transmitarray into the laminated glass structure as a solution to the penetration loss problem. In order to maintain the structure of the existing laminated glass and to incorporate the characteristics of the transmitarray, the transmitarray structure was inserted between the PVB films [9], as shown in Fig. 3. After dividing the PVB film in the existing laminated glass in half, two layers of silver with a Jerusalem cross pattern structure were inserted between them and polyethylene terephthalate (PET) film was inserted between the pattern structures. The role of the PET film is to provide a wide range of phase shifts by spacing the two metal layers. The reason that this PET film is used instead of conventional PVB film is related to the fabrication process, which is described in detail in Section V. The dielectric constant of PET film is 3.4 and the loss tangent is 0.002. The metal pattern structure was set to 1 μm thickness in consideration of the skin depth effect seen at 38.5 GHz. The metal pattern of UCs is shown in Fig. 4. The Jerusalem cross pattern was adopted because the window is intended to be used in a vehicle. To secure maximum transparency, the Jerusalem cross structure with the smallest area, about 10% of the UC area, is used. In addition, by unifying the width of the trace to 100 μm, the minimum processable thickness, transparency was only minimally impaired. This shape is applicable to both horizontal and vertical polarizations because of its symmetry. Although indium–tin oxide has the best-known transparency,

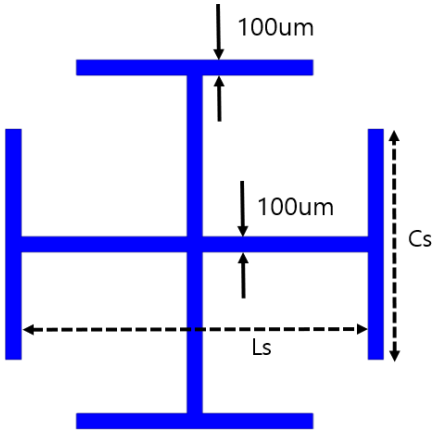

Fig. 4. Jerusalem cross shape used in the silver pattern of the UC shown in Fig. 3.

TABLE II

DIMENSION, PHASE SHIFT, AND IL OF UCS AT 38.5 GHZ WHEN A PLANE WAVE IS NORMALLY INCIDENT

UC#	Ls (mm)	Cs (mm)	Phase shift (°)	IL (dB)
1	1.8	0.4	-87	1.49
2	1.8	0.5	-108	0.98
3	1.8	0.7	-128	0.68
4	1.8	0.9	-145	0.65
5	1.8	1.4	-170	0.79
6	2.4	1.6	-191	1.17
7	2.4	1.7	-210	1.29

it exhibits low durability and discoloration when stacked to 1 μm thickness. Therefore, silver was used for the pattern structure. Figs. 5 and 6 show S_{21} parameters and phase shifts, respectively, when a plane wave is normally incident on seven types of UCs at 38.5 GHz. The detailed information is given in Table II. All UCs show less than 1.5 dB IL at 38.5 GHz. This is an improvement of about 1 dB from the 2.45 dB IL as shown in Table I for conventional laminated glass. The phase variation for shaping the beam is 123°. Table III shows the insertion losses and phase shifts for each UC, with the TE-polarization plane wave incidence, as a function of several incident angles. In almost all cases, insertion losses of less than 1.5 dB are shown. However, unlike conventional laminated glass shown in Fig. 1, it is difficult to identify the dependency between IL and incident angle for the UCs due to the parasitic element generated by subarms of the metal pattern whose length is represented by Cs in Fig. 4. It can also be seen that even if the incident angle increases up to 30°, the phase shift range is maintained over a range greater than 100° [10]–[12].

B. Proposed Design of the Transmitarray

In this section, we describe the design of the transmitarray realized by constructing an array of the UCs designed in Section III-A. The transmitarray is designed to focus millimeter waves on a specific region to improve communication

TABLE III

IL AND PHASE SHIFT OF UCS IN FIGS. 3 AND 4 AND TABLE II AT 38.5 GHZ, AS A FUNCTION OF SEVERAL INCIDENT ANGLES

Incident angle [°] (TE-pol)	10		20		30	
UC#	IL (dB)	Phase shift (°)	IL (dB)	Phase shift (°)	IL (dB)	Phase shift (°)
1	1.42	-87	2.13	-81	1.54	-93
2	0.88	-90	1.12	-100	0.91	-93
3	0.8	-109	0.67	-121	0.74	-111
4	0.96	-120	0.64	-132	0.85	-122
5	1.51	-148	0.84	-162	1.3	-152
6	1.54	-168	0.98	-181	1.36	-172
7	1.19	-192	0.96	-203	1.11	-194

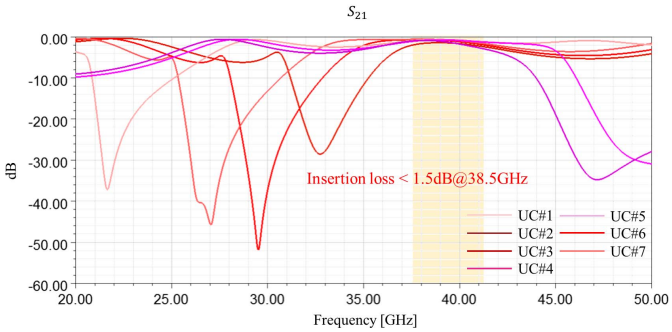

Fig. 5. S_{21} for seven types of UCs at 38.5 GHz when a plane wave is normally incident.

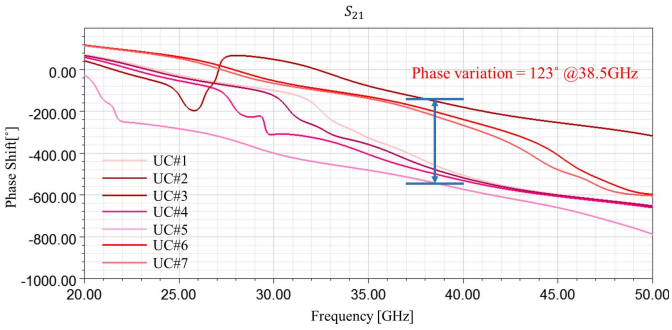

Fig. 6. Phase shift for seven types of UCs at 38.5 GHz when a plane wave is normally incident.

performance. The distance from the base station to the vehicle is generally large. Thus, the communication signal received at the side glass of the vehicle can be expressed as a plane wave. When the plane wave passes through the transmitarray, it directs signals to a specific location, as shown in Fig. 7, where communication is frequently generated.

The transmitarray proposed in this article is located in the vehicle passenger side window. As shown in Fig. 8, the distance from the side glass of the vehicle to the vehicle seat

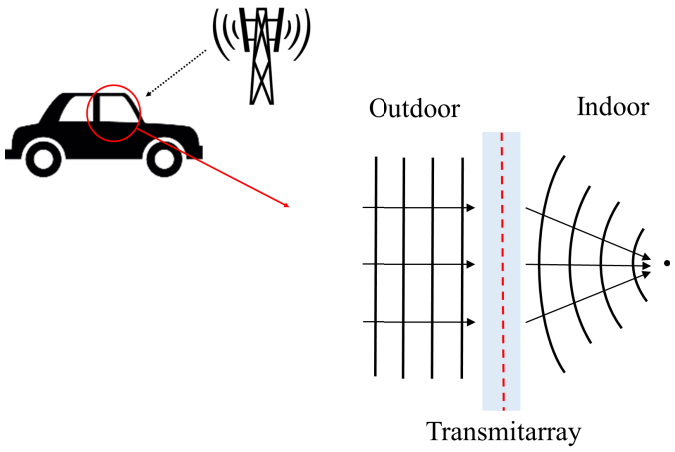

Fig. 7. Plane wave penetrating into an automobile through the transmitarray.

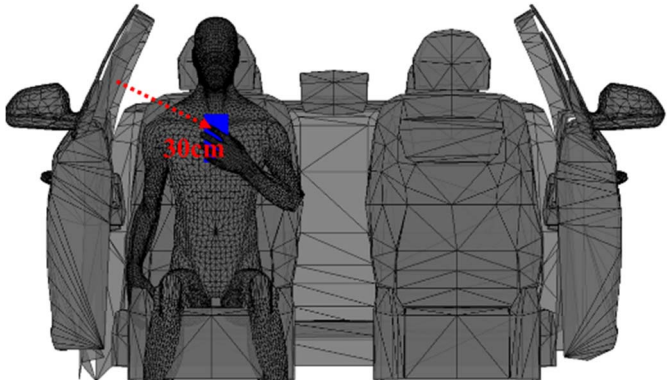

Fig. 8. Distance from the vehicle side window to the seat position.

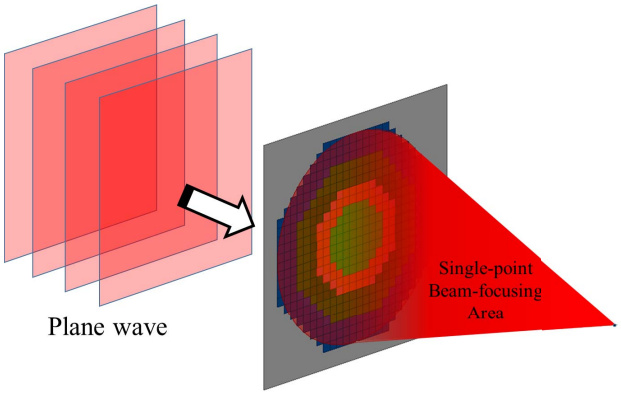

Fig. 9. Single-point beam-focusing area of conventional transmitarray.

is approximately 30 cm. Therefore, the transmitarray should be designed to have a focal length of 30 cm.

The transmitarray is designed by utilizing its reciprocal characteristics. The purpose of the conventional transmitarray is to convert the spherical wave radiated from the antenna into a plane wave to improve the gain. Conversely, as shown in Fig. 9, if a plane wave is incident on the conventional transmitarray, it is transformed into a single-point focus converging wave. On the other hand, the transmitarray proposed

TABLE IV

NUMBERED ZONE, NUMBER OF CASCADED UCS, SELECTED UC#, REQUIRED PHASE SHIFT IN THE MIDDLE OF EACH ZONE, PHASE SHIFT OF SELECTED UC, AND IL OF SELECTED UC OF THE TRANSMITARRAY IN FIG. 10 AT 38.5 GHZ

Zone #	Number of cascaded UCs	Selected UC#	Required phase shift in the middle of each zone [°]	Phase shift of selected UC [°]	IL of selected UC [dB]
1	8	7	-210	-210	1.29
2	4	6	-170	-191	1.17
3	2	5	-137	-170	0.79
4	1	4	-117	-145	0.65
5	2	3	-95	-128	0.68
6	1	2	-71	-108	0.98
7	5	1	-17	-87	1.49
8	7	7	-244	-210	1.29
9	1	6	-138	-191	1.17
10	1	4	-108	-145	0.65
11	1	3	-79	-128	0.68
12	1	7	-48	-210	1.29
13	2	1	0	-87	1.49
14	4	7	-259	-210	1.29

in this article is designed to form an aerial focus converging wave rather than a single-point focus converging wave. The transmitarray structure and its intended beam focusing area are shown in Fig. 10. The transmitarray is a vertically symmetrical and horizontally invariable structure. In the middle of the transmitarray, the UCs are arranged so that the phase is lagging, and the phase is leading closer to the edge portion. Table IV presents the numbered zones, the number of cascaded UCs, selected UC#, required phase shift in the middle of each zone, and phase shift/IL of the selected UC of the transmitarray in Fig. 10, at 38.5 GHz.

As shown in Fig. 10, the proposed transmitarray is a rectangular transmitarray with a 1-D structure, rather than the elliptic transmitarray with a 2-D structure, and can be applied with various incident angles [13]. Since it is composed of the same UCs in the horizontal direction, the transmitarray can operate on plane waves incident at various azimuth angles. On the other hand, the function of the transmitarray will be difficult to achieve if the plane wave is incident at various elevation angles. However, the millimeter wave incident from the base station to the vehicle through the line-of-sight (LOS) path will have a very long propagation distance. Thus, the elevation angle of the incident wave will be close to 0°. In conclusion, as shown in Fig. 10, the rectangular transmitarray with identical UCs arranged in the horizontal direction constitutes the optimal design. The size of the transmitarray is 20 cm × 20 cm and this is the maximum size of our benchtop fabricated sample. This arbitrarily chosen size can be of greater length in either direction. Ideally, a wide phase shift range of 360° is desired, but many practical constraints, such as available fabrication process/condition and geometrical features, limit

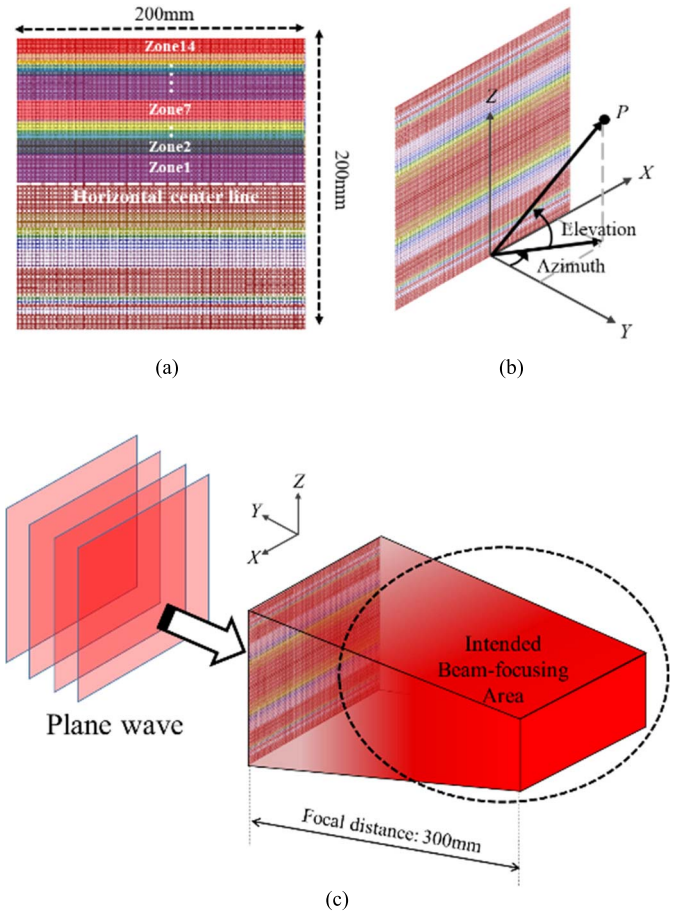

Fig. 10. Proposed transmitarray structure and its intended beam-focusing area. (a) Zone distribution. (b) Axis setting. (c) Intended beam focusing area.

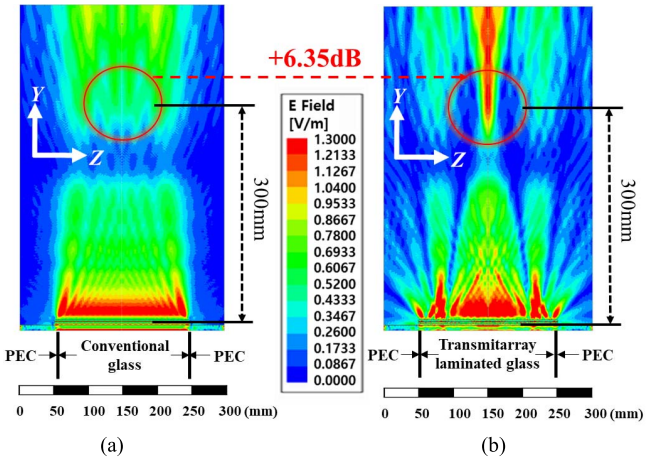

Fig. 11. HFSS simulation results. (a) Conventional laminated glass and (b) proposed transmitarray laminated glass; for a normally incident plane wave.

the realizable phase shift range in actual systems. This article first validates the operation feasibility of the window glass-embedded laminated transmitarray under actual fabrication conditions and laminated glass structure limiting the phase shift range into 123°. This practical background aspect has already been known and stated in the literature where various beam shaping functionalities and performance were able to be achieved within limited phase shift range [9], [14]–[17]. Fig. 11 shows that this limited transmitarray design still allows for the field enhancement in the intended manner.

Fig. 11 shows the results of the HFSS simulation for normally incident plane waves propagating in the $+y$-axis direction from below the E-field plots of Fig. 11. Fig. 11(a) shows the result of 20 cm $\times$ 20 cm conventional laminated glass and Fig. 11(b) shows the result of the proposed transmitarray laminated glass where both sizes of the transmitarray and glass are 20 cm $\times$ 20 cm. The plane outside the area where the proposed transmitarray laminated glass exists is filled with the perfect electric conductor (PEC) boundary, ignoring the effects of the fields penetrating the glass beyond the transmitarray to identify the performance of the proposed transmitarray itself. Similarly, for the conventional laminated glass scenario in Fig. 11(a), the plane outside the area where the conventional laminated glass exists is filled with the PEC boundary to assess the performance under the same conditions. Conventional and transmitarray laminated glass and the PEC boundary are located at the bottom of the E-field plots of Fig. 11, and except this area, free space is extended infinitely. The field intensity is increased by up to 6.35 dB at a distance of about 30 cm from the glass when the transmitarray is incorporated. The distance of 30 cm is the same with the assumed distance from the side glass of the vehicle to the vehicle seat, as shown in Fig. 8, where communication is mainly performed. This means that the main field intensity increase is successfully achieved at the area where communication most frequently occurs (i.e., area that communication devices in user's hand are mainly located when communication occurs). Approximately at 23 cm away from the window, there is a null of the field, both with transmitarray and without transmitarray. This is because, in the simulation, the glass does not extend infinitely, so diffraction occurs when a plane wave hits the edges of the glass and PEC plate. This results in destructive interference, resulting in null. The focal area is quite small vertically, about 1–3 cm in the z-axis direction, because the size of the transmitarray is not wide enough due to the limitation of our benchtop fabricated sample. However, the presented results confirmed the usefulness of the proposed window-embedded transmitarray topology, demonstrating its capability to manipulate the enhanced area vertically or horizontally. If the proposed transmitarray topology embedded in the laminated glass can be applied for the whole area of the window through mass production, the design freedom in controlling the enhanced area can be further increased. Stability for wide variation of the incidence angle can also be achieved using this design freedom because the focal area itself can be enlarged along the horizontal axis.

Fig. 12 shows the simulation results of the proposed transmitarray laminated glass for plane waves incident at various elevation angles. Similar to Fig. 11, the transmitarray laminated glass and the PEC boundary are located at the bottom of the E-field plots, and except for this area, free space is extended infinitely. The incident plane wave approaches from below the E-field plots. We simulated only for the two split

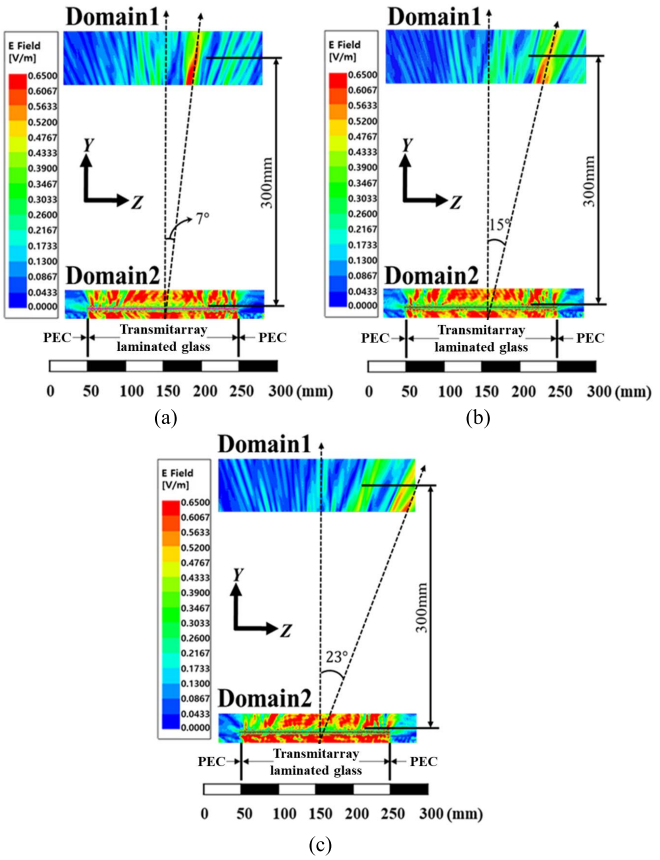

Fig. 12. HFSS simulation results of the proposed transmitarray laminated glass for plane waves incident at (a) 10°, (b) 20°, and (c) 30° elevation angles. Tilting angles are 7°, 15°, and 23°.

domains (i.e., domains 1 and 2 shown in Fig. 12) due to the tremendous computing and time loads in simulating the whole area. However, it is sufficient to identify the trends. As the incident elevation angle of the incident wave increases, the intensity of the transmitted electric field decreases. In addition, the tilting angle is smaller than the incident elevation angle. Also, sidelobes occur and there are two reasons for this. The first cause of the sidelobe occurrence is that diffraction occurred at edges of the transmitarray laminated glass and PEC plate. Sidelobes generated by this diffraction may be inevitable unless the size of the transmitarray laminated glass is infinity. Even if the transmitarray laminated glass is applied to the real vehicle, diffraction will occur at the edges of the metal vehicle frame and transmitarray laminated glass. The second cause of the sidelobe occurrence is the phase shift range limitation of the proposed transmitarray (i.e., 123°). This limitation creates a mismatch between the ideal UC arrangement with 360° phase shift range and the actual arrangement in this article as shown in Table IV, leading to the sidelobes. Sidelobes generated due to this phase shift range limitation can be interpreted as products of the practical constraints of the actual system.

IV. Ray-Tracing Simulation Scenario and Environment

In order to predict the effect of the transmitarray laminated glass proposed in Section III on the interior propagation

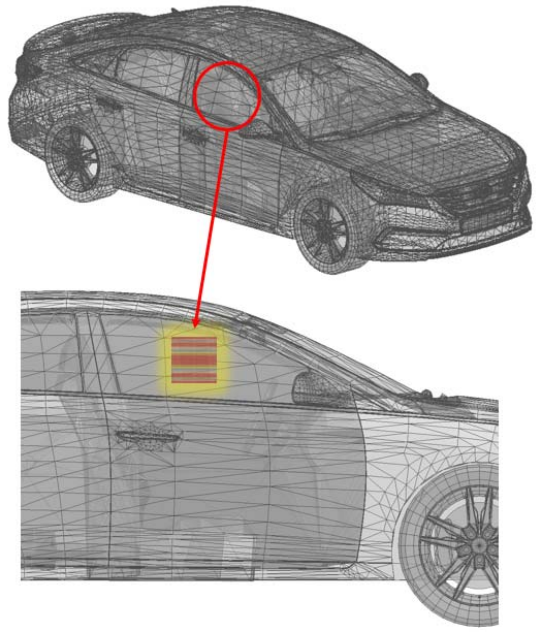

Fig. 13. Automobile CAD file to be used for the ray-tracing simulation and position of the proposed transmitarray.

TABLE V
Material Properties of the Automobile Interior in Fig. 13

Structure	Glass	Seat	Dash-board	Door skin	B-pillar trim
Dielectric constant	4.7	1.14	2.46	2.86	2.12
Conductivity	0.0325	0.0002	0.0025	0.0029	0.0003

environment of the vehicle, simulations using the ray-tracing numerical method suitable for massive space electromagnetic waves analysis were utilized. This simulation method supports multiple reflections, refractions, and diffractions. Basically, reflection and refraction follow Snell's law. However, for a material that has conductivity larger than zero, nonuniform plane wave theory is applied to reflection and refraction [18]. Consequently, high accuracy is assured, even if the simulation scenario includes materials with significant conductivities. Diffraction is applied using the uniform geometrical theory of diffraction (UTD) for fields contributed by wedge diffraction [19].

Fig. 13 shows the Hyundai Sonata (2015) computer-aided design (CAD) file, which was used for the simulation. Also, it shows the relative size of the proposed transmitarray, which is shown in Fig. 10, for the vehicle window There is a total of 60 000 triangle meshes. The interior properties of the vehicle to be used in the simulation are summarized in Table V.

The transmitarray is to be inserted at a position in the center of the passenger side laminated glass window. In the simulation, we compare existing conventional laminated glass and transmitarray laminated glass proposed in this article to determine their effects on the indoor propagation environment when a signal enters the interior of the car. In the car CAD file,

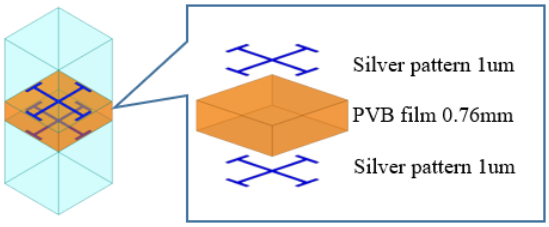

Fig. 14. Structure of the initial transmitarray laminated glass design.

the structure of the transmitarray is not implemented. Therefore, the propagation characteristics of the waves transmitted to the transmitarray will be determined with the results of the HFSS simulation in Section III. This information determines the characteristics of the ray, including penetration losses, phase shifts, and refraction angles. In Section V, we will compare the results of the ray-tracing simulation with the actual measurements.

V. Fabrication and Comparison Between Simulation and Measured Results

A. Fabrication

Fig. 14 shows the structure of the initial transmitarray laminated glass design. This transmitarray laminated glass was first designed with the insertion of metallic layers on the front and back of PVB films used in conventional laminated glass structures and without the use of PET films. However, the PVB film has an uneven surface that is not suitable for inserting a thin metallic layer with a thickness of 1 μm. Moreover, PVB films are opaque before processing the laminated glass. Therefore, it is difficult to align the metallic layers on the front and back of the film. For this reason, we adopted a structure with metal surfaces on the front and back of a transparent and smooth PET film, and we insert this between PVB films, as in Fig. 3. The microelectrical-mechanical systems (MEMS) process was used to coat the periodic structure of the metal on the front and back of the PET. Automotive glass, consisting of two 2.1 mm-thick glass layers with a PVB film between them, is processed at about 140° centigrade and 14 bar pressure. The transmitarray laminated glass proposed in this article is manufactured with the same process used in manufacturing the actual automotive glass.

Fig. 15 shows the Jerusalem cross pattern etched with silver on the front and back of the 450 μm PET film, which exhibits high transparency. The hand behind the structure is clearly visible due to the small occupation area of the silver pattern corresponding to about 10% of the UC area. Fig. 16 shows the result of completing the laminated glass process by inserting the PET film processed as in Fig. 15 into the center of the PVB film. The size of the laminated glass is 70 cm $\times$ 80 cm, and the PET is located in the center.

B. Measurement of Insertion Loss Due to Conventional Laminated Glass

Fig. 17 shows a schematic of an experimental environment for measuring the IL due to the conventional laminated glass shown in Fig. 1. A horn antenna (24–45 GHz) was used, and a vector network analyzer was used to measure the S_{21} parameters. The results for S_{21} parameters in the presence or absence of a 70 cm $\times$ 80 cm conventional laminated glass located about 30 cm from one side of the antenna are shown in Fig. 18. At 38.5 GHz, the IL due to the conventional laminated glass is about 4 dB. It is expected that the difference between the HFSS simulation result in Fig. 2 and the actual measurement in Fig. 18 is because

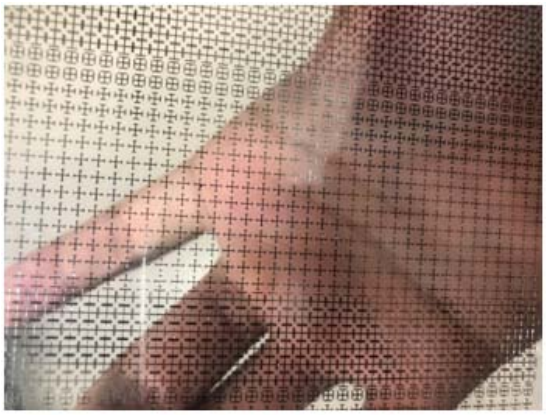

Fig. 15. Jerusalem cross pattern etched with silver on the front and back of the PET film.

Fig. 16. Laminated glass with the PET film of Fig. 15 inserted.

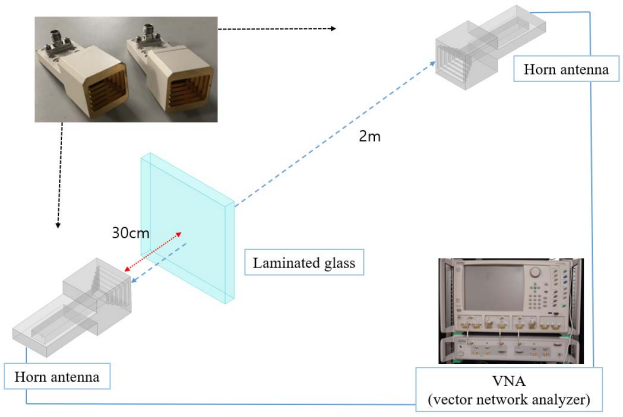

Fig. 17. Schematic of experimental environment for measuring the IL due to the conventional laminated glass shown in Fig. 1.

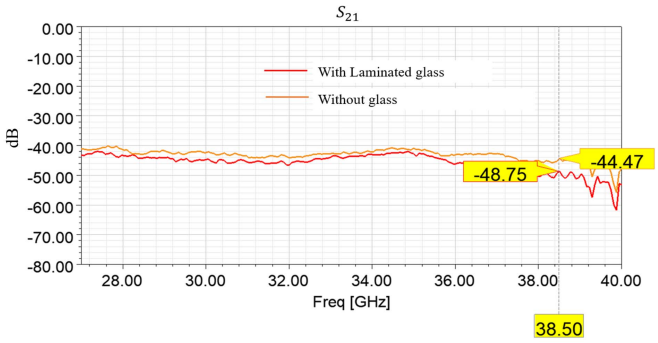

Fig. 18. Measurement results of the S_{21} of the conventional laminated glass shown in Fig. 1.

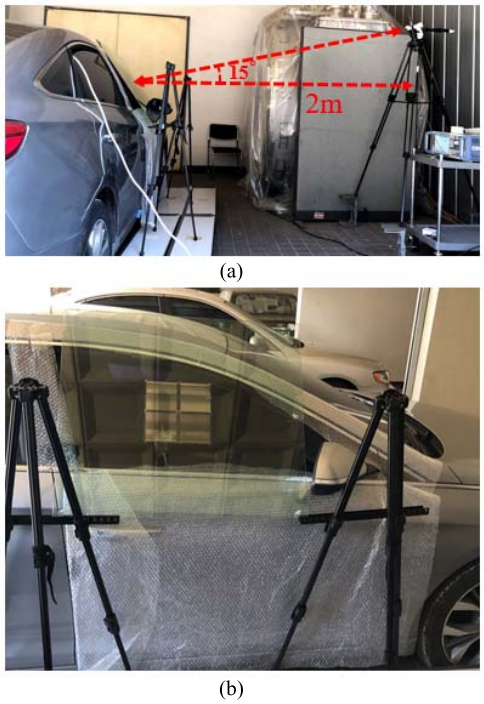

Fig. 19. Measurement setup of the proposed transmitarray laminated glass and lab equipment. (a) Overall view. (b) Setup of the transmitarray laminated glass.

the loss tangents of glass, PVB, and PET film are changed due to the MEMS process at 140° centigrade and 14 bar pressure. Another expected reason of the difference is that a perfect plane wave is used in HFSS simulation, while the horn antenna, which is 2 m apart away from the conventional laminated glass, was used in the actual measurement, as shown in Fig. 17. The IL becomes larger at the higher frequencies, that is, the IL is increased for higher frequency bands.

C. Comparison of Ray-Tracing Simulation and Measurement Results for Transmitarray Laminated Glass Applied to a Vehicle

Figs. 19 and 20 show the measurement setup for the transmitarray laminated glass applied to a vehicle. In order to allow the wave to enter the transmitarray in the normal direction, the transmitter (Tx) antenna was positioned at 0° azimuth and

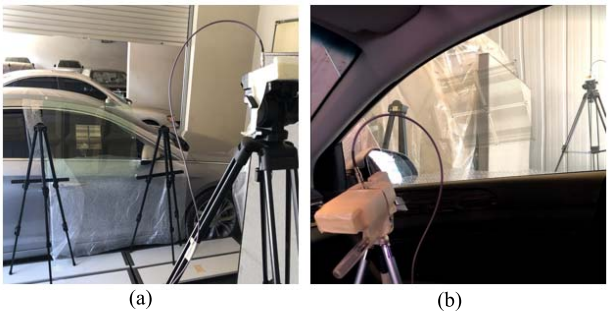

Fig. 20. Measurement setup of (a) Tx antenna and (b) Rx antenna.

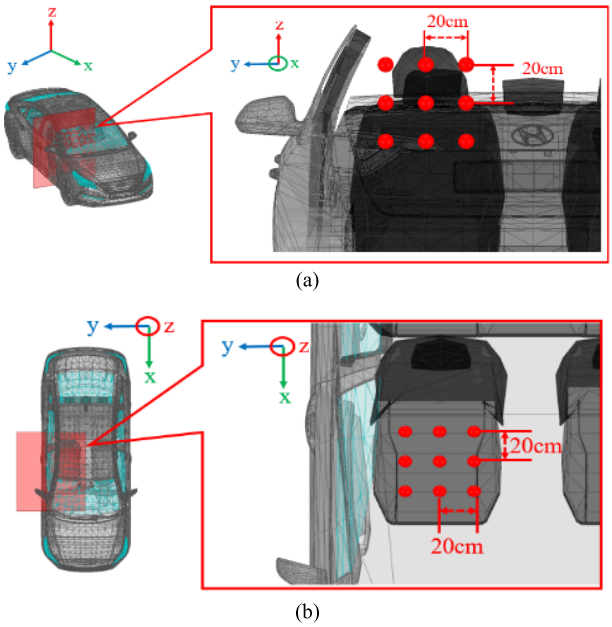

Fig. 21. 27 measuring points of the Rx antenna. (a) Front view. (b) Top view.

15° elevation (i.e., 0° elevation for the transmitarray laminated glass). The Tx antenna was placed at a distance about 2 m from the transmitarray laminated glass in a horizontal direction to produce a plane wave effect with the same phase. The receiver (Rx) antenna location was varied with positions on the passenger seat. The signal generator was connected to the Tx antenna, and the spectrum analyzer was connected to the Rx antenna. Also, we measured the increased amount of the field intensity due to the proposed transmitarray by comparing the case of using the proposed window with the case of the conventional existing window. The vehicle used in the experiment is the Hyundai Sonata (2015), for which the CAD file was used in the ray-tracing simulation. The position at which the signal is concentrated by the transmitarray corresponds to the headrest portion of the passenger seat, one of the positions from which communication is frequently generated. Therefore, the position of the Rx antenna is located at 27 points spaced 20 cm up, down, left, and right and at a height of about 80 cm from the bottom of the passenger seat, as shown in Fig. 21.

The measurement results and the ray-tracing simulation results were compared for all 27 points. The simulation

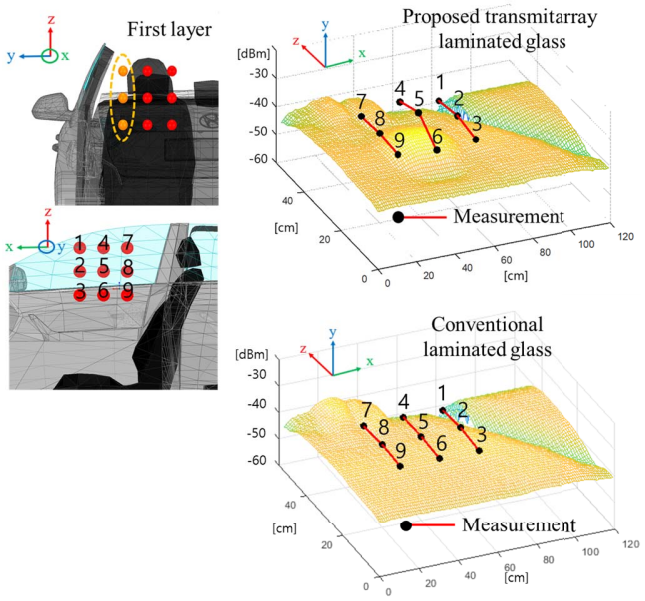

Fig. 22. Comparison of measurement and simulation results in the first layer, which is the closest layer to the window.

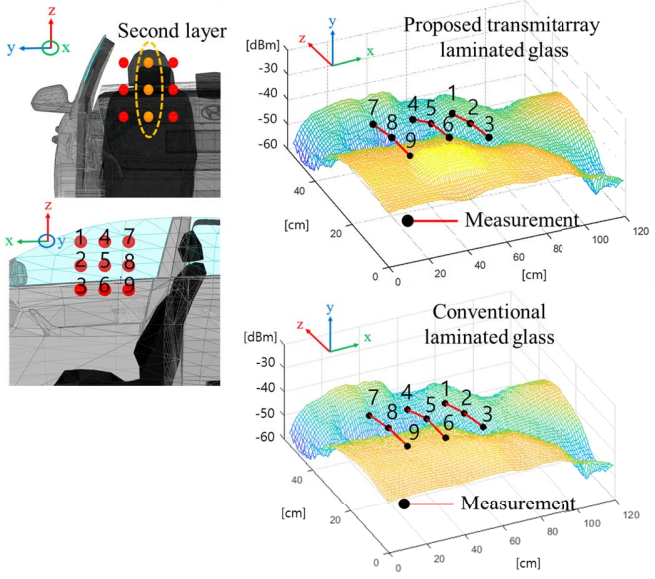

Fig. 23. Comparison of measurement and simulation results in the second layer, which is the middle layer.

allowed plane waves with an azimuth of 0° and an elevation of 15° to have the incident wave enter the transmitarray perpendicularly, as in the measurement environment. The simulation allowed six reflections, two transmissions, and one diffraction. The simulation and measurement results were divided into three XZ-planes and were compared.

In Figs. 22–24 and Tables VI–VIII, the field intensity is increased at specific locations. The first layer in Fig. 22 shows the highest field intensity increase of about 4.6 dB at point 5. Figs. 23 and 24 show the highest field intensity increase at point 6, about 4.3 and 3.5 dB, respectively. The reason why

TABLE VI

COMPARISON OF MEASUREMENT AND SIMULATION RESULTS IN THE FIRST LAYER IN FIG. 22, WHICH IS THE CLOSEST LAYER TO THE WINDOW

Simulation			
#	Conventional Window [dBm]	Proposed Window [dBm]	Field Intensity Increase [dB]
1	-43.88	-43.49	0.39
2	-42.82	-42.32	0.5
3	-43.81	-43.87	-0.06
4	-43.49	-41.49	2
5	**-43.18**	**-38.51**	**4.67**
6	-43.78	-44.49	-0.71
7	-43.94	-43.92	0.02
8	-43.13	-43.10	0.03
9	-43.67	-43.67	0
Measurement			
#	Conventional Window [dBm]	Proposed Window [dBm]	Field Intensity Increase [dB]
1	-45.32	-45.37	-0.05
2	-45.13	-44.94	0.19
3	-45.57	-45.26	0.31
4	-44.46	-45.40	-0.94
5	**-45.00**	**-40.45**	**4.55**
6	-45.01	-44.83	0.18
7	-44.71	-45.72	-1.01
8	-45.22	-45.99	-0.77
9	-44.38	-46.21	-1.83

the measured field enhancement is lower than the simulation result in Fig. 11 may be the undesired multipath effect (i.e., a destructive interference at this case) caused by the application of the transmitarray laminated glass to the devised vehicle experiment. Although the field enhancement with the vehicle used for the experiments in this article is lower than when the transmitarray laminated glass is located at the center of the PEC boundary, as shown in Fig. 11, the field enhancement can be increased if the transmitarray laminated glass is applied to customized vehicle windows. The reason why the field enhancement does not occur in the horizontal plane, but only at one point is that the size of the transmitarray is not large enough. This is the limitation of our benchtop fabricated sample. However, the size of the transmitarray can be enlarged in a horizontal direction by mass production, resulting in a horizontally wide field enhancement. The field intensity also decreases, such as at point 4 of the third layer in Fig. 24. This sacrifice at the periphery results from concentrating the signal at a specific location. The average error rate obtained from

TABLE VII

COMPARISON OF MEASUREMENT AND SIMULATION RESULTS IN THE SECOND LAYER IN FIG. 23, WHICH IS THE MIDDLE LAYER

Simulation			
#	Conventional Window [dBm]	Proposed Window [dBm]	Field Intensity Increase [dB]
1	-49.34	-49.04	0.3
2	-44.34	-44.34	0
3	-41.39	-41.32	0.07
4	-48.00	-48.00	0
5	-42.85	-40.96	1.89
6	**-42.25**	**-38.00**	**4.25**
7	-46.63	-46.63	0
8	-43.17	-43.17	0
9	-42.01	-42.01	0
Measurement			
#	Conventional Window [dBm]	Proposed Window [dBm]	Field Intensity Increase [dB]
1	-51.33	-50.82	0.51
2	-49.12	-48.52	0.6
3	-45.02	-46.89	-1.87
4	-52.2	-50.52	1.68
5	-50.85	-53.76	-2.91
6	**-49.28**	**-45.00**	**4.28**
7	-52.93	-51.63	1.3
8	-48.67	-50.15	-1.48
9	-47.71	-50.45	-2.74

TABLE VIII

COMPARISON OF MEASUREMENT AND SIMULATION RESULTS IN THE THIRD LAYER IN FIG. 24, WHICH IS THE FARTHEST LAYER TO THE WINDOW

Simulation			
#	Conventional Window [dBm]	Proposed Window [dBm]	Field Intensity Increase [dB]
1	-52.84	-52.30	0.54
2	-51.88	-51.29	0.59
3	-45.29	-44.48	0.81
4	-46.83	-48.24	-1.41
5	-53.01	-53.24	-0.23
6	**-43.05**	**-39.19**	**3.86**
7	-48.58	-48.84	-0.26
8	-52.11	-52.11	0
9	-42.91	-42.92	-0.01
Measurement			
#	Conventional Window [dBm]	Proposed Window [dBm]	Field Intensity Increase [dB]
1	-54.84	-55.34	-0.5
2	-54.68	-54.27	0.41
3	-48.49	-46.12	2.37
4	-49.83	-52.14	-2.31
5	-54.61	-55.28	-0.67
6	**-47.45**	**-44.08**	**3.37**
7	-53.10	-52.34	0.76
8	-55.61	-54.81	0.8
9	-46.88	-46.92	-0.04

the difference between the simulation and the measured result is about 7%. This is considered sufficient to demonstrate the trends.

To this point, the experiment has involved a plane wave incident on the transmitarray in the normal direction. Table IX compares the increased amount of the field intensity in the simulation and the measured results when the wave is incident at various elevation and azimuth angles. The position of the Rx antenna is point 5 of the first layer in Fig. 22. Since the transmitarray adopts a 1-D structure in which the same UCs are arranged in the horizontal direction, it shows a constant gain value for various azimuth incident angles. On the other hand, the gain decreases sharply as the incident elevation angle increases. Over the incident elevation angle of 20°, the proposed window shows lower performance than that of conventional laminated glass. It is because the vertical size of the transmitarray itself is not large enough due to the limitation of our benchtop fabricated sample, resulting in vertically narrow area where field intensity enhancement occurs. If the proposed transmitarray topology embedded in the laminated glass can be applied for the entire area of the window through mass production, the beamforming area itself

TABLE IX

INCREASED AMOUNT OF FIELD INTENSITY FOR VARIOUS INCIDENT ANGLES

	Elevation angle			
	0 °	**10 °**	**20 °**	**30 °**
Field Intensity Increase [dB] (Simulation)	4.67	2.0	-1.2	-2.0
Field Intensity Increase [dB] (Measurement)	4.55	1.2	-3.3	-5.1
	Azimuth angle			
	0 °	**10 °**	**20 °**	**30 °**
Field Intensity Increase [dB] (Simulation)	4.67	4.67	4.42	4.33
Field Intensity Increase [dB] (Measurement)	4.55	4.5	4.52	4.25

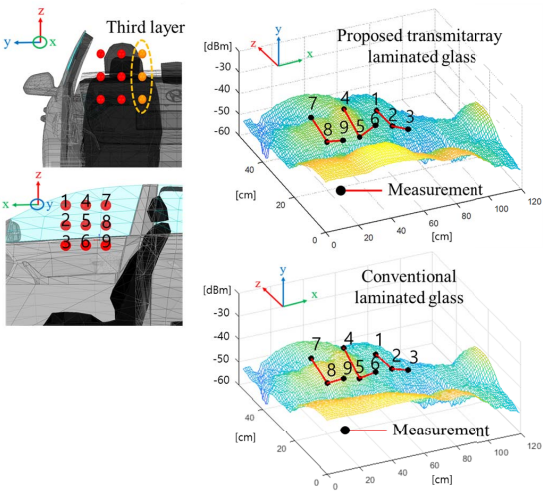

Fig. 24. Comparison of measurement and simulation results in the third layer, which is the farthest layer to the window.

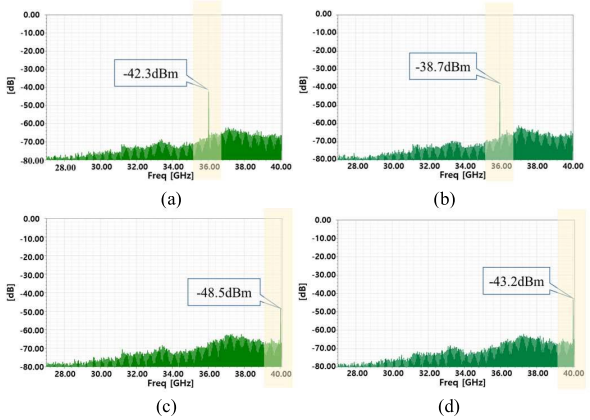

Fig. 25. Measurement results at point 5 of the first layer in Fig. 22 for (a) conventional laminated glass (36 GHz), (b) proposed transmitarray laminated glass (36 GHz), (c) conventional laminated glass (40 GHz), and (d) proposed transmitarray laminated glass (40 GHz).

will be sufficiently wide in the vertical direction. Thus, even if the incident elevation angle is changed, the field intensity enhancement will be maintained more constantly.

The simulations and measurements discussed in the previous part were conducted at a single frequency of 38.5 GHz. Fig. 25 shows the measurement results at 36 and 40 GHz. The measurement setup is identical to Figs. 19 and 20. Also, the Rx antenna is located at point 5 of the first layer in Fig. 22. The measured results show the field intensity increases of 3.6 and 5.3 dB at 36 and 40 GHz, respectively. The average increase of the field intensity is about 3 dB from 36 to 40 GHz.

VI. Conclusion

Both FEM and ray-tracing-based simulations were used to identify and improve high penetration losses caused by conventional vehicle glass. The laminated glass window embedded transmitarray proposed in this article can overcome this problem. The proposed transmitarray laminated glass reduces IL and improves signal strength at the target area, where communication is mainly performed, through beam shaping function. Also, this transmitarray laminated glass shows high commercial possibilities as it has adopted the glass structure used in actual vehicles. Likewise, the transmitarray is inserted inside the glass. Thus, there is no foreign texture on the surface. In addition, the Jerusalem cross shape metal pattern of the UC was implemented using silver in this article due to the limitation of our benchtop sample. If nanoweb material, which is not only conductive but also transparent, is used for the metal pattern, the transmitarray laminated glass will have far superior transparency.

In addition to vehicles, the transmitarray laminated glass can be applied to various locations where windows are used, such as offices surrounded by glass windows. Also, various arrangements of UCs can be used to make the desired beam shaping function.

In conclusion, high penetration loss in the millimeter-wave frequency band is one of the major problems currently being addressed. The automobile laminated glass window embedded transmitarray proposed in this article will be one way to solve the problem.

References

[1] D. Ha, D. Choi, H. Kim, J. Kum, J. Lee, and Y. Lee, "Passive repeater for removal of blind spot in NLOS path for 5G fixed wireless access (FWA) system," in *Proc. IEEE Int. Symp. Antennas Propag. USNC/URSI Nat. Radio Sci. Meeting*, Jul. 2017, pp. 2049–2050.

[2] J. Kim and J. Oh, "Liquid-crystal-embedded aperture-coupled microstrip antenna for 5G applications," *IEEE Antennas Wireless Propag. Lett.*, vol. 19, no. 11, pp. 1958–1962, Nov. 2020.

[3] W. A. Awan, S. I. Naqvi, A. H. Naqvi, S. M. Abbas, A. Zaidi, and N. Hussain, "Design and characterization of wideband printed antenna based on DGS for 28 GHz 5G applications," *J. Electromagn. Eng. Sci.*, vol. 21, no. 3, pp. 177–183, Jul. 2021.

[4] F. Hossain, T. Geok, T. Rahman, M. Hindia, K. Dimyati, and A. J. S. Abdaziz, "Indoor millimeter-wave propagation prediction by measurement and ray tracing simulation at 38 GHz," *Symmetry*, vol. 10, no. 10, p. 464, Oct. 2018.

[5] N. Jamaly, D. Scanferla, C. Genoud, and H. Lehmann, "Analysis and measurement of penetration loss for train wagons with coated vs uncoated windows," in *Proc. 12th Eur. Conf. Antennas Propag. (EuCAP)*, Apr. 2018, pp. 1–5.

[6] K. Sarabandi, J. Oh, L. Pierce, K. Shivakumar, and S. Lingaiah, "Lightweight, conformal antennas for robotic flapping flyers," *IEEE Antennas Propag. Mag.*, vol. 56, no. 6, pp. 29–40, Dec. 2014.

[7] E. Kim, S. T. Ko, Y. J. Lee, and J. Oh, "Millimeter-wave tiny lens antenna employing U-shaped filter arrays for 5G," *IEEE Antennas Wireless Propag. Lett.*, vol. 17, no. 5, pp. 845–848, May 2018.

[8] A. A. Dewani, S. G. O'Keefe, D. V. Thiel, and A. Galehdar, "Window RF shielding film using printed FSS," *IEEE Trans. Antennas Propag.*, vol. 66, no. 2, pp. 790–796, Feb. 2018.

[9] J. Oh, "Millimeter-wave thin lens employing mixed-order elliptic filter arrays," *IEEE Trans. Antennas Propag.*, vol. 64, no. 7, pp. 3222–3227, Jul. 2016.

[10] J. Oh, M. Thiel, W. Hong, and K. Sarabandi, "Indoor wave propagation measurements and modeling for evaluation of coverage enhancement using a repeater system," in *Proc. IEEE Antennas Propag. Soc. Int. Symp.*, Jun. 2009, pp. 1–4.

[11] J. Oh, G. Z. Hutcheson, F. Aryanfar, W. Hong, and Y. J. Lee, "Planar beam steerable lens antenna system using non-uniform feed method," in *Proc. IEEE Antennas Propag. Soc. Int. Symp. (APSURSI)*, Jul. 2014, pp. 651–652.

[12] J. Oh, G. Z. Hutcheson, W. Hong, and Y. J. Lee, "Planar lens using mixed-order spatial elliptic filter," in *Proc. IEEE Antennas Propag. Soc. Int. Symp. (APSURSI)*, Jul. 2014, pp. 735–736.

[13] I. Yoon and J. Oh, "Millimeter-wave thin lens using multi-patch incorporated unit cells for polarization-dependent beam shaping," *IEEE Access*, vol. 7, pp. 45504–45511, 2019.

[14] J. Oh, "Millimeter-wave short-focus thin lens employing disparate filter arrays," *IEEE Antennas Wireless Propag. Lett.*, vol. 15, pp. 1446–1449, 2016.

[15] H. Kaouach, L. Dussopt, R. Sauleau, and T. Koleck, "Design and demonstration of 1-bit and 2-bit transmit-arrays at X-band frequencies," in *Proc. Eur. Microw. Conf. (EuMC)*, Roma, Italy, Sep./Oct. 2009, pp. 918–921.
[16] B. Rana, I.-G. Lee, and I.-P. Hong, "Experimental characterization of 2×2 electronically reconfigurable 1 bit unit cells for a beamforming transmitarray at X band," *J. Electromagn. Eng. Sci.*, vol. 21, no. 2, pp. 153–160, Apr. 2021.
[17] J. H. Yoon and Y. J. Yoon, "Bandwidth enhancement of single-layer microstrip reflectarrays with multi-dipole elements," *J. Electromagn. Eng. Sci.*, vol. 19, no. 2, pp. 130–139, Apr. 2019.
[18] R. D. Radcliff and C. A. Balanis, "Modified propagation constants for nonuniform plane wave transmission through conducting media," *IEEE Trans. Geosci. Remote Sens.*, vol. GRS-20, no. 3, pp. 408–411, Jul. 1982.
[19] P. Bernardi, R. Cicchetti, and O. Testa, "A three-dimensional UTD heuristic diffraction coefficient for complex penetrable wedges," *IEEE Trans. Antennas Propag.*, vol. 50, no. 2, pp. 217–224, Feb. 2002.

Seokyeon Hong (Member, IEEE) received the B.S. degree in electrical and electronic engineering from Yonsei University, Seoul, South Korea, in 2018, and the M.S. degree in electrical and computer engineering from Seoul National University, Seoul, in 2020.

His research interests include display antenna design and metamaterial-based transmitarray antenna for 5G communications.

Yongwan Kim (Member, IEEE) received the B.S. degree in electrical engineering from Chungnam National University, Daejeon, South Korea, in 2019. He is currently pursuing the Ph.D. degree with Seoul National University, Seoul, South Korea.

His current research interests include ray-tracing EM analysis technique and EMI/EMC for 5G communication.

Jungsuek Oh (Senior Member, IEEE) received the B.S. and M.S. degrees from Seoul National University, Seoul, South Korea, in 2002 and 2007, respectively, and the Ph.D. degree from the University of Michigan, Ann Arbor, MI, USA, in 2012.

From 2007 to 2008, he was with Korea Telecom, Seongnam-si, South Korea, as a Hardware Research Engineer, working on the development of flexible RF devices. From 2013 to 2014, he was a Staff RF Engineer with Samsung Research America, Dallas, TX, USA, working as a Project Leader for the 5G/millimeter-wave antenna system. From 2015 to 2018, he was a Faculty Member with the Department of Electronic Engineering, Inha University, Incheon, South Korea. He is currently an Associate Professor with the Department of Electrical and Computer Engineering, Seoul National University. He has published more than 60 technical journal articles and conference papers. His research interests include mmWave metasurface/lens beam focusing/shaping techniques, antenna miniaturization for integrated systems, and radio propagation modeling for complex scenarios.

Dr. Oh has served as a TPC Member and as the Session Chair for numerous conferences, such as IEEE AP-S/USNC-URSI, International Symposium on Antennas and Propagation, KIEES: Korean Institute of Electromagnetic Engineering and Science (ISAP), and KIEES Conferences, where his team has been awarded honorably. He was a recipient of the 2011 Rackham Predoctoral Fellowship Award at the University of Michigan. He has served as a Technical Reviewer for the IEEE TRANSACTIONS ON ANTENNAS AND PROPAGATION, IEEE ANTENNAS AND WIRELESS PROPAGATION LETTERS, and so on.